Biodesign

pISSN 2288-6982 | eISSN 2288-7105
https://doi.org/10.34184/kssb.2023.11.4.59

ARTICLE P 59-65

Crystal structure of *Bacillus subtilis* glyceraldehyde-3-phosphate dehydrogenase GapB

Pawan Dahal[1], Deepak Pathak[1] and Eunju Kwon[2,3,*]

[1]College of Pharmacy, Yeungnam University, Gyeongsan 38541, Republic of Korea
[2]Division of Life Science, Gyeongsang National University, Jinju 52828, Republic of Korea
[3]Research Institute of Molecular Alchemy, Gyeongsang National University, Jinju 52828, Republic of Korea
*Correspondence: eunjukwon@gnu.ac.kr

Glyceraldehyde 3-phosphate dehydrogenase (GAPDH) catalyzes the interconversion of glyceraldehyde 3-phosphate and 1,3-diphosphoglycerate during glycolysis and gluconeogenesis. In most organisms, a single GAPDH is responsible for the reaction. However, *Bacillus subtilis* has two isoforms of this enzyme, namely, GapA and GapB, each of which catalyzes the reaction in the opposite direction. GapA uses NAD^+ as a cofactor, whereas GapB prefers $NADP^+$. In this study, we report the crystal structure of GapB at 2.3 Å resolution. X-ray diffraction of GapB crystal was observed up to 2.0 Å resolution, and its structure was determined using molecular replacement. Its overall fold and quaternary structure (a homo-tetramer) were similar to that of the reported GAPDHs. The S-loop was missing because of the absence of the $NADP^+$.

INTRODUCTION

Glycolysis is a metabolic process that occurs in most organisms, where one glucose molecule is converted into two pyruvate molecules through 10 sequential enzymatic reactions (Scrutton and Utter, 1968). The sixth reaction of glycolysis is the process that converts glyceraldehyde 3-phosphate (G3P) into 1,3-bisphosphoglycerate (1,3-BPG) (Figure 1A) (Harris and Waters, 1976). This process is catalyzed by glyceraldehyde-3-phosphate dehydrogenase (GAPDH). During this reaction, the aldehyde group of G3P is oxidized to a carboxyl group, and NAD^+ is reduced to NADH. Phosphate is then covalently attached to the oxidized G3P.

GAPDH catalyzes the interconversion between G3P and 1,3-BPG depending on substrate concentration. G3P is oxidized to 1,3-BPG by GAPDH during glycolysis, whereas 1,3-BPG is reduced to G3P by the same enzyme during gluconeogenesis (Harris, 1976) (Figure 1A). A single GAPDH mediates this interconversion in many organisms. However, two or more GAPDHs have been identified in plants (Petersen et al., 2003) and some species of prokaryotes, such as cyanobacteria (Koksharova et al., 1998), archaea (Brunner et al., 2001; Ito et al., 2012; Tastensen and Schonheit, 2018), and non-photosynthetic bacteria (Purves et al., 2010). In prokaryotic species containing two GAPDH genes, GapA catalyzes the oxidation of G3P to 1,3-BPG during glycolysis, while GapB catalyzes the reverse reaction during gluconeogenesis (Koksharova et al., 1998; Brunner et al., 2001; Purves et al., 2010; Ito et al., 2012; Tastensen and Schonheit, 2018).

Bacillus subtilis, a model organism for gram-positive bacteria, also possesses two GAPDHs: BsGapA and BsGapB (Kunst et al., 1997). BsGapA is a classical NAD^+-dependent GAPDH that catalyzes the1,3-BPG production during glycolysis, whereas BsGapB is an $NADP^+$-dependent enzyme that mediates the reverse reaction during gluconeogenesis. GAPDH contains characteristic residues for cofactor binding. BsGapA contains Asp34, Leu190, and Pro191 for NAD^+ binding. BsGapB contains Ala34, Asn190, and Pro191 for $NADP^+$ binding (Corbier et al., 1990; Clermont et al., 1993; Fillinger et al., 2000). The folding of BsGapB is assisted by the YjoB chaperone in *B. subtilis* (Kwon et al., 2022).

Since the first GAPDH structure was determined (Moras et al., 1975), many GAPDH structures from approximately 70 species have been reported. NAD^+-dependent GAPDH structures have been extensively studied, while $NADP^+$-dependent GAPDH structures have been relatively less studied. Herein, the crystal structure of $NADP^+$-dependent BsGapB is determined at 2.3 Å resolution and compared with previously known structures.

MATERIALS AND METHODS

Protein preparation

BsGapB was prepared as described previously (Kwon et al., 2022). In brief, the *B. subtilis* gapB gene (residues 1-340) was amplified using a polymerase chain reaction from the genomic DNA of the *B. subtilis* strain 168. The gene was inserted into the pETDuet-1 vector (Merck Millipore, Billerica, MA, USA) modified with DNA encoding 6×His-thioredoxin (Trx) and a tobacco etching virus (TEV) protease cleavage sequence to express the 6×His-Trx-BsGapB protein. The plasmid was introduced

into the *E. coli* strain BL21-star (DE3) (Thermo Fisher Scientific, Waltham, MA, USA), and the cells were cultured in Luria Bertani medium at 37°C. When the optical density at 600 nm reached 0.6-0.7, the protein expression was induced by adding 0.4 mM isopropyl β-D-1-thiogalactopyranoside. The cells were then cultured for 24 h at 20°C and harvested through centrifugation at 3,000 ×*g* for 10 min at 4°C. The harvested cells were resuspended in buffer A (20 mM HEPES pH 7.5, 0.2 M NaCl, and 5% (v/v) glycerol) and lysed by sonication. Cell lysates were treated with DNase I and RNase A (10 μg/ml each; Roche, Basel, Switzerland) for 30 min on ice and clarified through centrifugation at 20,000 ×*g* for 30 min at 4°C.

BsGapB was purified using immobilized metal affinity chromatography and size-exclusion chromatography (SEC). Cell lysates were loaded onto a 5-ml HisTrap nickel-chelating column (Cytiva, Marlborough, MA, USA), and proteins bound to the resin were eluted through a linear gradient of 0.08-1.0 M imidazole on an AKTA-FPLC system (Cytiva). Fractions containing 6×His-Trx-BsGapB were pooled and incubated with TEV protease at 4°C to separate the 6×His-Trx tag from BsGapB. After cleavage, the protein solution was dialyzed against buffer A and passed through a HisPur Ni-NTA resin (Thermo Fisher Scientific) to remove the 6×His-Trx tag. BsGapB was further purified by SEC using a Superdex 200 preparatory grade column (Cytiva) equilibrated with buffer B (20 mM HEPES pH 7.5, 50 mM NaCl, and 5% (v/v) glycerol).

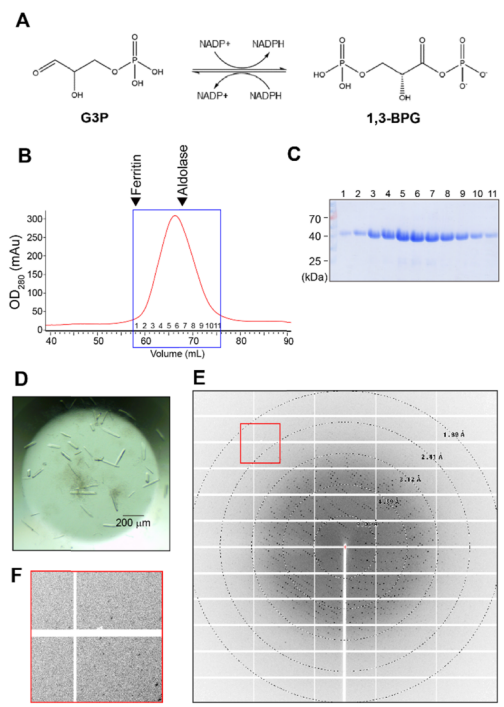

FIGURE 1 I Protein purification and crystallization of BsGapB. (A) Diagram showing interconversion between G3P and 1,3-BPG by GAPDH. (B) The UV profile of size-exclusion chromatography showing BsGapB elution. Molecular weight of proteins is: ferritin, 440 kDa; aldolase, 158 kDa; GapB, 37.6 kDa. (C) SDS-PAGE showing size-exclusion chromatography eluates in the blue box of (B). (D) Rod-shaped crystals of BsGapB. (E) An X-ray diffraction image of the BsGapB crystal. (F) Magnified diffraction image showing the reflections in the red box of (E).

Crystallization, data collection, and structure determination

BsGapB crystals suitable for X-ray diffraction grew in micro-batch plates (Hampton Research, Aliso Viejo, CA, USA) at 20°C. The crystallization drop was set up by mixing 1 μl BsGapB (11.75 mg/ml) and 1 μl crystallization solution under AI's oil layer (Hampton Research). Crystals grew completely within 2 weeks in the crystallization solution containing 20.1% (v/v) 2-methyl-2,4-pentanediol, 10.05% (w/v) polyethylene glycol 8000, 0.1 M $CaCl_2$, and 0.1 M sodium acetate/acetic acid pH 5.5 (Rigaku, Tokyo, Japan). For cryo-protection, 0.5 μl of 100% glycerol was directly added to the crystallization drop. Single crystals were

TABLE 1 I Data collection and refinement statistics

Data collection	
Diffraction source	PAL/PLS BEAMLINE 11C
Wavelength (Å)	0.9794
Temperature (K)	100
Space group	$P6_222$
a, *b*, *c* (Å)	102.60, 102.60, 111.08
α, β, γ (°)	90.00, 90.00, 120.00
Resolution range (Å)	88.85–2.30 (2.38–2.30)
R_{meas} (%)	14.7 (79.7)
$< I/\sigma(I) >$	16.0 (4.5)
Completeness (%)	100.0 (100,0)
Redundancy	18.9 (19.0)
Mosaicity (°)	0.68
Total no. of reflections	302,108 (28,816)
No. of unique reflections	15,937 (1,519)
Refinement	
Resolution range (Å)	88.85-2.30 (2.48–2.30)
R_{work}/R_{free} (%)	19.4/25.1 (17.5/24.6)
No. of non-H atoms	
Protein	745
Water	137
Total	882
R.m.s. deviations	
Bonds (Å)	0.005
Angles (°)	0.772
Average *B* factors (Å^2)	12.4
Protein	10.8
Water	20.9
Ramachandran plot	
Most favored (%)	97.7
Allowed (%)	2.3
Cruickshank DPI	0.034

Values for the outer shell are provided in parentheses.

then picked up using dual-thickness micro loops (MiTeGen, Ithaca, NY, USA) and rapidly frozen in liquid nitrogen.

Diffraction data were collected at PLS II-BL11C (Beamline 11C, Pohang Light Source II, South Korea) (Park et al., 2017). The data were indexed, integrated, and scaled using MOSFLM (Battye et al., 2011) and AIMLESS (Evans and Murshudov, 2013). The crystal structure of BsGapB was determined using the molecular replacement method in Phaser (McCoy et al., 2007). The AlphaFold model structure of BsGapB (AlphaFold ID: O34425-F1) was used as the template for molecular replacement (Jumper et al., 2021). Model building and structure refinement were performed using COOT (Emsley et al., 2010) and Phenix.refine (Afonine et al., 2012; Liebschner et al., 2019).

Figures were drawn using ChemDraw (Revvity Signals Software, Waltham, MA, USA) and PyMOL (Schrodinger, 2015). Diffraction images were prepared using ADXV (Scripps Research Institute, La Jolla, CA, USA). The InterPro database was used for protein classification and domain organization (Paysan-Lafosse et al., 2023). Structure alignment and protein-protein interactions were analyzed using the DALI server (Holm and Rosenstrom, 2010) and PISA (Krissinel and Henrick, 2007). The final coordinate and structure factor of BsGapB were deposited in the Protein Data Bank (PDB ID: 8WWZ).

RESULTS AND DISCUSSION

Crystallographic data collection and structure determination of BsGapB

Although hundreds of GAPDH structures from approximately 70 species have been deposited in the PDB, the crystal structure of BsGapB has not yet been reported. Full-length BsGapB was purified and crystallized to determine its crystal structure. The 6×His-Trx-BsGapB was expressed in *E. coli* at 20°C. The protein was purified using immobilized metal affinity chromatography, and the 6×His-Trx tag was removed by treatment of TEV protease, after which it was passed through the nickel-chelating resin. BsGapB was further purified by SEC using a Superdex 200 preparatory grade column (Figure 1B and 1C). In SEC, BsGapB was observed at elution volume of approximately 65 ml, wherein it was estimated to be a tetramer (Figure 1B). BsGapB was crystallized into a rod-shape using 2-methyl-2,4-pentanediol and polyethylene glycol 8000 as precipitants (Figure 1D). The crystal was exposed to a micro-focusing X-ray source, and reflections were observed up to 2.0 Å resolution (Figure 1E and 1F). The collected diffraction data were processed at 2.3 Å resolution (Table 1). A total of 302,108 reflections were observed, which were merged to 15,937 unique reflections with an R_{merge}/R_{pim} of 0.143/0.033. The dataset completeness was 100.0%. The crystal belonged to the hexagonal space group $P6_222$ with unit cell parameters of a = 102.60 and c = 111.08 (Å) (Table 1). The Matthews coefficient (V_M) was calculated to be 2.25 $Å^3$/Da, assuming that one BsGapB was in the crystallographic asymmetric unit. This value corresponded to a solvent content of 45.3%.

The crystal structure of BsGapB was determined using the molecular replacement method. For the structure determination, an alpha-fold model of BsGapB (AlphaFold ID: O34425-F1) was used as the template for molecular replacement (Jumper et al., 2021). The asymmetric unit of the crystal contained one

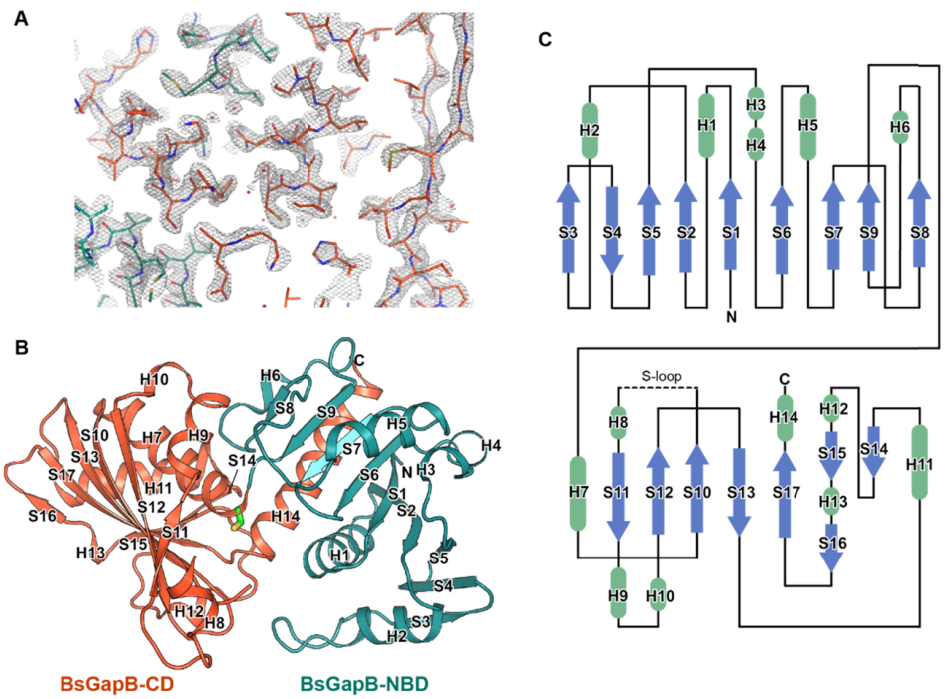

FIGURE 2 I Crystal structure of BsGapB monomer. (A) 2*Fo-Fc* electron density map shown at a 2.0 σ contour level. (B) Crystal structure of BsGapB monomer. NADP-binding domain (NBD; residues 2-150) and catalytic domain (CD; residues 151-337) are colored in teal and orange, respectively. Secondary structures are designated as H1-H14 for helices and S1-S17 for strands. A catalytic residue (Cys152) is shown as a green stick model. (C) Topology model of BsGapB monomer.

BsGapB chain modeled at residues 2-182 and 194-337. The final structure was refined at 2.3 Å resolution with an R_{work}/R_{free} value of 19.4/25.1%. (Table 1 and Figure 2A).

Crystal structure of BsGapB monomer

GAPDH is composed of an N-terminal NAD(P)$^+$-binding domain (NBD) and a C-terminal catalytic domain (CD) (Moras et al., 1975; Olsen et al., 1975). In the crystal structure of BsGapB, residues 2-150 and 151-337 corresponded to the NBD and CD of GAPDH, respectively (Figure 2). BsGapB-NBD formed a Rossmann fold with a core β-sheet and peripheral helices. The core β-sheet contained six parallel β-strands arranged in the order: S5, S2, S1, S6, S7, and S9. The helices in the NBD (H1, H2, H3/H4, H5, and H6) were inserted between the strands (S1 and S2, S2 and S5, S5 and S6, S6 and S7, and S7 and S9 strands, respectively) and were placed on both sides of the core β-sheet (Figure 2B and 2C). β-hairpin (S3 and S4) and S8 strand extended this Rossmann fold of BsGapB-NBD by forming β-sheet hydrogen bonds with S5 and S9, respectively (Figure 2C). BsGapB-CD formed an α/β fold composed of a central β-sheet and peripheral helices (Figure 2B and 2C). In the central β-sheet of BsGapB-CD, three β-strands (S10, S12, and S13) formed a psi-loop motif as a β-sheet core. The S11 strand and the remaining β-strands (S14-S17) extended the psi-loop motif by forming β-sheet hydrogen bonds with S12 and S13, respectively (Figure 2C). The C-terminal helix H14 bound to the concave groove in the core β-sheet of the NBD, contributing to the formation of a globular and stable monomer (Figure 2B).

Structural homology searches showed that BsGapB shared an overall fold with GAPDHs in a wide range of species. *Bacillus*

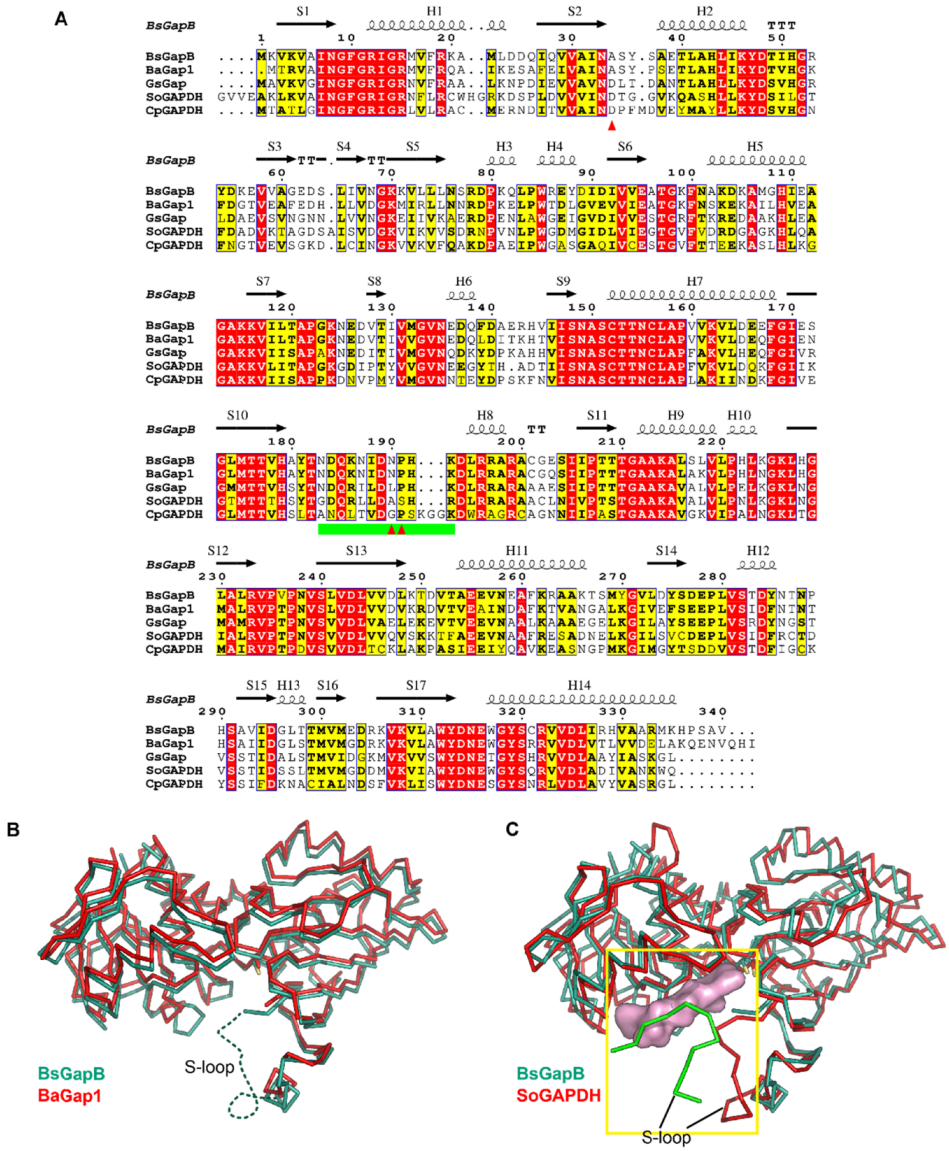

FIGURE 3 I Structural comparison of BsGapB with GAPDHs. (A) Sequence alignment of BsGapB and other GAPDHs. Coils and arrows represent helices and strands of BsGapB, respectively. Red triangles and a green bar indicate signature residues (D34, L190, and P191) and S-loop, respectively. The sequence information and species abbreviations are as follows: *Bacillus anthracis* Gap1 (UniProt ID: A0A348AAL1): BaGap1; *Geobacillus stearothermophilus* Gap (UniProt ID: P00362): GsGap; *Spinacia oleracea* GAPDH (UniProt ID: P19866): SoGAPDH; *Cryptosporidium parvum* GAPDH (UniProt ID: Q7YYQ9): CpGAPDH. The sequence identity of BaGap1, GsGap, SoGAPDH, and CpGAPDH with BsGapB is 72.3, 61.5, 54.8, and 45.7%, respectively. (B) The superimposed Cα trace models of BsGapB (teal) and BaGap1 (red; PDB ID 4DIB). The teal dotted line indicates the flexible S-loop of BsGapB. The RMSD value between BsGapB and BaGap1 is 0.9 Å for 322 Cα atoms. (C) The superimposed Cα trace models of BsGapB (teal) and SoGAPDH (red; PDB ID 1RM5). The green Cα trace represents the S-loop from a neighboring subunit of *S. oleracea* GAPDH. The pink surface model represents NADP$^+$ bound to SoGAPDH. The RMSD value between BsGapB and SoGAPDH is 1.4 Å for 322 Cα atoms.

anthracis apo-Gap1 (PDB ID: 4DIB), *Geobacillus stearothermophilus* NAD^+-bound Gap (PDB ID: 1DBV) (Didierjean et al., 1997), *Spinacia oleracea* $NADP^+$-bound GAPDH (PDB ID: 1RM5) (Sparla et al., 2004), and *Cryptosporidium parvum* apo-GAPDH (PDB ID: 1VSU) (Cook et al., 2009) were superimposed onto BsGapB, with root mean square deviation values of 0.9, 1.0, 1.4, and 1.2 Å for 322 Cα atoms, respectively. This indicates that the overall structure of GapB was well-aligned with GAPDH structures, except for the missing loop (Figure 3).

In the crystal structure of BsGapB, residues 183-193 were not visible (Figure 3B). The missing residues corresponded to the S-loop, which mediates $NAD(P)^+$ binding (Cook et al., 2009). The S-loop is flexible in the apo-GAPDH structure, whereas it is fixed in the $NAD(P)^+$-bound GAPDH structures by interacting with $NAD(P)^+$ (Figure 3B and 3C). Thus, a major difference in the presence and absence of the cofactor was observed in the S-loop.

Crystal structure of BsGapB tetramer

GAPDHs form a tetramer arranged by three 2-fold axes (222 symmetry) (Harris and Waters, 1976), and BsGapB was estimated to be a tetramer by SEC (Figure 1B). Although the BsGapB monomer was found in the asymmetric unit, it was predicted to form a stable homo-tetramer in the PISA analysis (Krissinel and Henrick, 2007). BsGapB tetramer was assembled with 222 symmetry like other GAPDHs (Figure 4A-D) (Biesecker et al., 1977; Sparla et al., 2004; Ferreira-da-Silva et al., 2006) and its extensive binding interfaces resulted in the surface burial of 27.8% (12,885 $Å^2$ in 46,360 $Å^2$) and significantly reduced ΔG (–76.6 kcal/mol). This shows that the BsGapB tetramer has the conserved quaternary structure of GAPDH.

BsGapB contains Ala34, Asn190, and Pro191 as the signature residues for $NADP^+$ binding. In the crystal structure of BsGapB superimposed with S. oleracea GAPDH, Ala34 was located close to $NADP^+$, and Asn190 and Pro191 in the S-loop were not visible (Figure 4E). Given that the S-loop of the neighboring subunit interacted with $NADP^+$ in the crystal structure of *S. oleracea* GAPDH tetramer, the S-loop of BsGapB appeared to be stabilized by interaction with $NADP^+$ in the neighboring subunit of the BsGapB oligomer (Figure 4E).

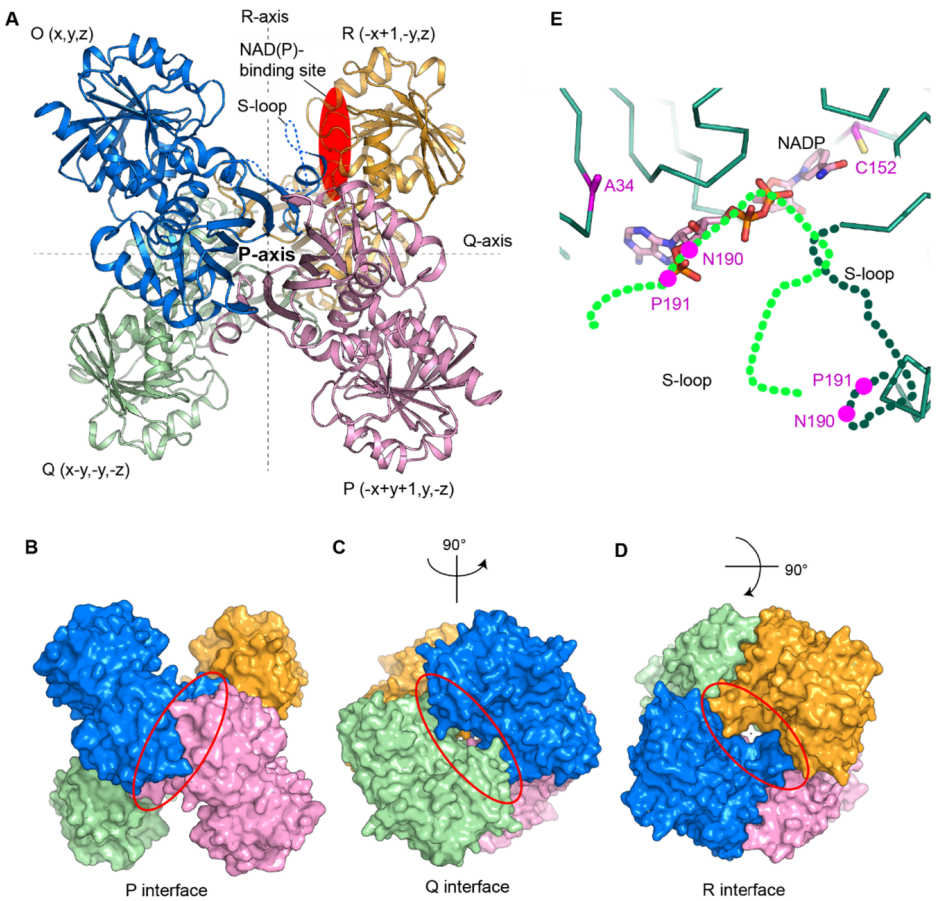

FIGURE 4 I Crystal structure of BsGapB tetramer. (A) Cartoon model of BsGapB tetramer. BsGapB tetramer is generated by three crystallographic 2-fold symmetry (P-, Q-, and R-axis). (B-D) Surface models showing three different binding interfaces of BsGapB tetramer. Red ovals indicate the binding interface for BsGapB tetramerization. (E) Signature residues (Ala34, Asn190, and Pro191) of BsGapB for $NADP^+$ binding. The teal and green dotted lines represent BsGapB S-loops from one subunit (teal) and the neighboring subunit (green). These S-loops were modeled using the crystal structure of SoGAPDH tetramer (PDB ID: 1RM5). The magenta circles highlight the signature residues for $NADP^+$ binding.

ACKNOWLEDGEMENTS

This research was supported by Learning & Academic research institution for Master's·PhD students, and Postdocs (LAMP) Program of the National Research Foundation of Korea (NRF) grant funded by the Ministry of Education (RS-2023-00301974).

CONFLICT OF INTEREST

The authors declare no competing interests.

Original Submission: Nov 6, 2023
Revised Version Received: Dec 5, 2023
Accepted: Dec 12, 2023

REFERENCES

Afonine, P.V., Grosse-Kunstleve, R.W., Echols, N., Headd, J.J., Moriarty, N.W., Mustyakimov, M., Terwilliger, T.C., Urzhumtsev, A., Zwart, P.H., and Adams, P.D. (2012). Towards automated crystallographic structure refinement with phenix.refine. *Acta Crystallogr D Biol Crystallogr* **68**, 352-367.

Battye, T.G., Kontogiannis, L., Johnson, O., Powell, H.R., and Leslie, A.G. (2011). iMOSFLM: a new graphical interface for diffraction-image processing with MOSFLM. *Acta Crystallogr D Biol Crystallogr* **67**, 271-281.

Biesecker, G., Harris, J.I., Thierry, J.C., Walker, J.E., and Wonacott, A.J. (1977). Sequence and structure of D-glyceraldehyde 3-phosphate dehydrogenase from Bacillus stearothermophilus. *Nature* **266**, 328-333.

Brunner, N.A., Siebers, B., and Hensel, R. (2001). Role of two different glyceraldehyde-3-phosphate dehydrogenases in controlling the reversible Embden-Meyerhof-Parnas pathway in Thermoproteus tenax: regulation on protein and transcript level. *Extremophiles* **5**, 101-109.

Clermont, S., Corbier, C., Mely, Y., Gerard, D., Wonacott, A., and Branlant, G. (1993). Determinants of coenzyme specificity in glyceraldehyde-3-phosphate dehydrogenase: role of the acidic residue in the fingerprint region of the nucleotide binding fold. *Biochemistry* **32**, 10178-10184.

Cook, W.J., Senkovich, O., and Chattopadhyay, D. (2009). An unexpected phosphate binding site in glyceraldehyde 3-phosphate dehydrogenase: crystal structures of apo, holo and ternary complex of Cryptosporidium parvum enzyme. *BMC Struct Biol* **9**, 9.

Corbier, C., Clermont, S., Billard, P., Skarzynski, T., Branlant, C., Wonacott, A., and Branlant, G. (1990). Probing the coenzyme specificity of glyceraldehyde-3-phosphate dehydrogenases by site-directed mutagenesis. *Biochemistry* **29**, 7101-7106.

Didierjean, C., Rahuel-Clermont, S., Vitoux, B., Dideberg, O., Branlant, G., and Aubry, A. (1997). A crystallographic comparison between mutated glyceraldehyde-3-phosphate dehydrogenases from Bacillus stearothermophilus complexed with either NAD+ or NADP+. *J Mol Biol* **268**, 739-759.

Emsley, P., Lohkamp, B., Scott, W.G., and Cowtan, K. (2010). Features and development of Coot. *Acta Crystallogr D Biol Crystallogr* **66**, 486-501.

Evans, P.R., and Murshudov, G.N. (2013). How good are my data and what is the resolution? *Acta Crystallogr D Biol Crystallogr* **69**, 1204-1214.

Ferreira-da-Silva, F., Pereira, P.J., Gales, L., Roessle, M., Svergun, D.I., Moradas-Ferreira, P., and Damas, A.M. (2006). The crystal and solution structures of glyceraldehyde-3-phosphate dehydrogenase reveal different quaternary structures. *J Biol Chem* **281**, 33433-33440.

Fillinger, S., Boschi-Muller, S., Azza, S., Dervyn, E., Branlant, G., and Aymerich, S. (2000). Two glyceraldehyde-3-phosphate dehydrogenases with opposite physiological roles in a nonphotosynthetic bacterium. *J Biol Chem* **275**, 14031-14037.

Harris, J.I., and Waters, M. 1 Glyceraldehyde-3-phosphate Dehydrogenase Ch.1 In: The Enzymes, (Academic Press, 1976), pp. 1-49.

Holm, L., and Rosenstrom, P. (2010). Dali server: conservation mapping in 3D. *Nucleic Acids Res* **38**, W545-W549.

Ito, F., Chishiki, H., Fushinobu, S., and Wakagi, T. (2012). Comparative analysis of two glyceraldehyde-3-phosphate dehydrogenases from a thermoacidophilic archaeon, Sulfolobus tokodaii. *FEBS Lett* **586**, 3097-3103.

Jumper, J., Evans, R., Pritzel, A., Green, T., Figurnov, M., Ronneberger, O., Tunyasuvunakool, K., Bates, R., Žídek, A., Potapenko, A., Bridgland, A., Meyer, C., Kohl, S.A.A., Ballard, A.J., Cowie, A., et al. (2021). Highly accurate protein structure prediction with AlphaFold. *Nature* **596**, 583-589.

Koksharova, O., Schubert, M., Shestakov, S., and Cerff, R. (1998). Genetic and biochemical evidence for distinct key functions of two highly divergent GAPDH genes in catabolic and anabolic carbon flow of the cyanobacterium Synechocystis sp. PCC 6803. *Plant Mol Biol* **36**, 183-194.

Krissinel, E., and Henrick, K. (2007). Inference of macromolecular assemblies from crystalline state. *J Mol Biol* **372**, 774-797.

Kunst, F., Ogasawara, N., Moszer, I., Albertini, A.M., Alloni, G., Azevedo, V., Bertero, M.G., Bessières, P., Bolotin, A., Borchert, S., Borriss, R., Boursier, L., Brans, A., Braun, M., Brignell, S.C., et al. (1997). The complete genome sequence of the gram-positive bacterium Bacillus subtilis. *Nature* **390**, 249-256.

Kwon, E., Dahal, P., and Kim, D.Y. (2022). Crystal structure and biochemical analysis suggest that YjoB ATPase is a putative substrate-specific molecular chaperone. *Proc Natl Acad Sci U S A* **119**, e2207856119.

Liebschner, D., Afonine, P.V., Baker, M.L., Bunkóczi, G., Chen, V.B., Croll, T.I., Hintze, B., Hung, L.W., Jain, S., McCoy, A.J., Moriarty, N.W., Oeffner, R.D., Poon, B.K., Prisant, M.G., Read, R.J., et al. (2019). Macromolecular structure determination using X-rays, neutrons and electrons: recent developments in Phenix. *Acta Crystallogr D Struct Biol* **75**, 861-877.

McCoy, A.J., Grosse-Kunstleve, R.W., Adams, P.D., Winn, M.D., Storoni, L.C., and Read, R.J. (2007). Phaser crystallographic software. *J Appl Crystallogr* **40**, 658-674.

Moras, D., Olsen, K.W., Sabesan, M.N., Buehner, M., Ford, G.C., and Rossmann, M.G. (1975). Studies of asymmetry in the three-dimensional structure of lobster D-glyceraldehyde-3-phosphate dehydrogenase. *J Biol Chem* **250**, 9137-9162.

Olsen, K.W., Moras, D., and Rossmann, M.G. (1975). Sequence variability and structure of D-glyceraldehyde-3-phosphate dehydrogenase. *J Biol Chem* **250**, 9313-9321.

Park, S.Y., Ha, S.C., and Kim, Y.G. (2017). The protein crystallography beamlines at the Pohang Light Source II. *Biodesign* **5**, 30-34.

Paysan-Lafosse, T., Blum, M., Chuguransky, S., Grego, T., Pinto, B.L., Salazar, G.A., Bileschi, M.L., Bork, P., Bridge, A., Colwell, L., Gough, J., Haft, D.H., Letunić, I., Marchler-Bauer, A., Mi, H., et al. (2023). InterPro in 2022. *Nucleic Acids Res* **51**, D418-D427.

Petersen, J., Brinkmann, H., and Cerff, R. (2003). Origin, evolution, and metabolic role of a novel glycolytic GAPDH enzyme recruited by land plant plastids. *J Mol Evol* **57**, 16-26.

Purves, J., Cockayne, A., Moody, P.C., and Morrissey, J.A. (2010). Comparison of the regulation, metabolic functions, and roles in virulence

of the glyceraldehyde-3-phosphate dehydrogenase homologues gapA and gapB in Staphylococcus aureus. *Infect Immun* **78**, 5223-5232.

Schrodinger, L. (2015). The PyMOL molecular graphics system, version 1.8.

Scrutton, M.C., and Utter, M.F. (1968). The regulation of glycolysis and gluconeogenesis in animal tissues. *Annu Rev Biochem* **37**, 249-302.

Sparla, F., Fermani, S., Falini, G., Zaffagnini, M., Ripamonti, A., Sabatino, P., Pupillo, P., and Trost, P. (2004). Coenzyme site-directed mutants of photosynthetic A4-GAPDH show selectively reduced NADPH-dependent catalysis, similar to regulatory AB-GAPDH inhibited by oxidized thioredoxin. *J Mol Biol* **340**, 1025-1037.

Tastensen, J.B., and Schonheit, P. (2018). Two distinct glyceraldehyde-3-phosphate dehydrogenases in glycolysis and gluconeogenesis in the archaeon Haloferax volcanii. *FEBS Lett* **592**, 1524-1534.